THE JOURNAL OF PHYSICAL CHEMISTRY Letters

pubs.acs.org/JPCL Letter

Application of First-Principles-Based Artificial Neural Network Potentials to Multiscale-Shock Dynamics Simulations on Solid Materials

Masaaki Misawa,* Shogo Fukushima, Akihide Koura, Kohei Shimamura, Fuyuki Shimojo, Subodh Tiwari, Ken-ichi Nomura, Rajiv K. Kalia, Aiichiro Nakano, and Priya Vashishta

Cite This: *J. Phys. Chem. Lett.* 2020, 11, 4536–4541

ABSTRACT: The use of artificial neural network (ANN) potentials trained with first-principles calculations has emerged as a promising approach for molecular dynamics (MD) simulations encompassing large space and time scales while retaining first-principles accuracy. To date, however, the application of ANN-MD has been limited to *near-equilibrium* processes. Here we combine first-principles-trained ANN-MD with multiscale shock theory (MSST) to successfully describe *far-from-equilibrium* shock phenomena. Our ANN-MSST-MD approach describes shock-wave propagation in solids with first-principles accuracy but a 5000 times shorter computing time. Accordingly, ANN-MD-MSST was able to resolve fine, long-time elastic deformation at low shock speed, which was impossible with first-principles MD because of the high computational cost. This work thus lays a foundation of ANN-MD simulation to study a wide range of far-from-equilibrium processes.

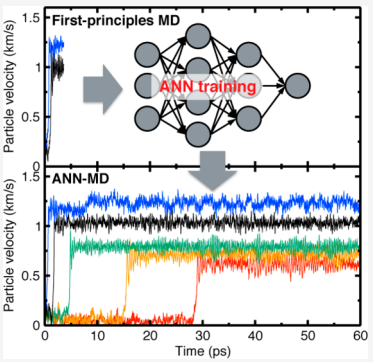

Investigating wave propagation properties and shock-wave-induced structural dynamics in earth-abundant materials is important not only for geodynamics research but also to understand material processes.[1−5] For example, it is reported that silica (SiO_2) transforms into the nanopolycrystalline form of stishovite, which is a high-pressure polymorph of silica, during high-pressure shock compression.[1] This nanopolycrystalline stishovite has been nominated for next-generation high-performance ceramics because of its high hardness and toughness.[6−9] To study the atomistic-scale dynamics in materials under such extreme conditions, molecular dynamics (MD) simulations exert great power because they are able to chase the atomic trajectories with extremely high time resolution (femtoseconds). In particular, the first-principles MD (FPMD) method based on density functional theory (DFT) calculations provides us great insight into microscopic mechanisms of such complex phenomena from the viewpoint of electronic states. To treat wave propagation or shock-induced chemistry or structural transformation in materials, Reed et al., proposed a multiscale nonequilibrium MD technique using the 1D Euler equation for compressible flow.[10] By the use of this multiscale shock technique (MSST), atomistic behaviors at the shock wavefront can be represented on long time scales. The combination of MSST with FPMD has succeeded in investigating mechanical responses, chemical reactions, phase transitions, and their anisotropy for various materials under shock compression.[11−13]

However, the computable space and time scales for FPMD simulations are limited to the order of several hundred atoms and tens of picoseconds because of its high computational cost. Therefore, shock-induced structural transformations or chemical reactions that require more than several tens of picoseconds (e.g., the previously mentioned formation of stishovite[1]) are difficult to investigate efficiently using the FPMD method. In order to solve this problem, many efforts have been made to extend the computable space and time scales by reducing computational cost while retaining the first-principles accuracy.[14−26] In this trend, recently the construction of empirical potentials based on artificial neural networks (ANNs) has attracted a lot of attention as a solution to the computational cost issue.[16−24] The fundamental idea of this method to use an ANN that has learned the correlation of the atomic configuration and potential energy of the system as an empirical potential energy function. If the learning has been effective enough, the computational cost of the MD simulation with the ANN potential (ANN-MD) is reduced to that of classical MD (CMD) level while the FPMD accuracy is retained, at least for the reference configuration. To construct an empirical potential using an ANN, the total energy of the system is defined as a sum of the atomic energies, and these atomic contributions are considered as output information on feed-forward neural

Received: February 28, 2020
Accepted: May 22, 2020
Published: May 22, 2020

https://dx.doi.org/10.1021/acs.jpclett.0c00637
J. Phys. Chem. Lett. 2020, 11, 4536–4541

networks (FFNNs). In addition to that, the Cartesian coordinates, which are obtained by first-principles calculations, are transformed into a set of basis functions that depict the local structural environment associated with each atom.[17] The basis function is defined as a set of atom-centered radial and angular functions that correspond to bond lengths and bond angles around an atom, respectively.[23,24] The ANN potentials constructed by this scheme have been used for wide range of systems and provided excellent results.[27−30] However, there is no precedent for the application to shock propagation simulations to date.

In this work, we have attempted to perform shock simulations using a first-principles-based ANN potential and to show that ANN potentials have a potential application to nonequilibrium MD simulations under extreme conditions. For the model system, α-quartz was employed, and the elastic deformation reaction under shock compression has been calculated. The shock-related quantities produced by the ANN potential were compared with FPMD results, and the quality and potential application to the shock simulation of the ANN potential were investigated. The main contribution of this paper is the first application of ANNs to far-from-equilibrium processes while retaining first-principles accuracy with applicability to much larger spatiotemporal scales. This is achieved by combining the ANN potential and MSST, with a specific illustrative application to shock-compressed quartz.

In order to obtain the first-principles-based atomistic behavior and prepare teaching data for learning of the ANN potential, shock simulations based on FPMD and MSST were performed for α-quartz. First, we prepared a hexagonal simulation cell consisting of 243 atoms ($Si_{81}O_{162}$), which corresponds to 3 × 3 × 3 lattice of the crystal unit cell of α-quartz. During MD simulations, periodic boundary conditions for all directions were applied to the simulation cell. Next, to create an initial configuration for the shock simulations, the crystal structure was relaxed by an FPMD simulation with the isothermal−isobaric (*NPT*) ensemble under ambient conditions during 1500 steps (1.82 ps). Then the shock simulations were carried out using MSST for various shock speeds with a range of 6.0 to 7.4 km/s. The shock direction was set to the [210] direction, which is perpendicular to the (100) plane of α-quartz (Figure 1). For each set of shock conditions, FPMD simulations were carried out until elastic or plastic deformation reactions were observed (at least 0.6 ps).

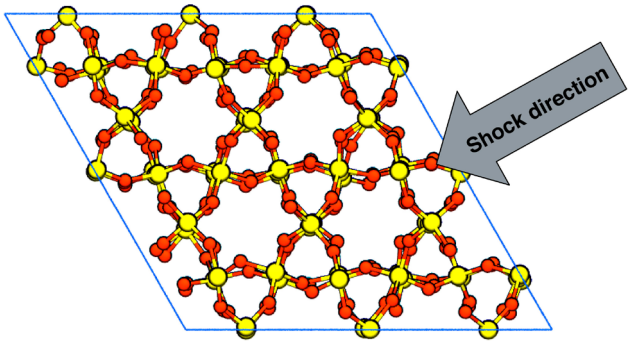

Figure 1. Schematic image of the shock-induced simulation. The yellow and red balls illustrate silicon and oxygen atoms, respectively. The blue line indicates the periodic boundary of the simulation cell. The shock wave is induced along the [210] direction, which is perpendicular to the (100) plane of α-quartz.

Using the ANN potential that was constructed on the basis of the FPMD simulation data, ANN-MD shock simulations were performed with the same simulation system as for the FPMD simulations. The time step, process to create the initial configuration, and shock direction were also the same as for the FPMD simulation. As the result of the shock simulation during 60.5 ps (50 000 steps) with the ANN potential, we observed elastic deformation behavior at shock speeds of 5.7−6.4 km/s. In order to compare the calculation speed and quality of the ANN potential, a traditional CMD simulation with an empirical interatomic pair potential was also performed. The setup procedures and simulation conditions were same as for the ANN-MD simulation. Information about the empirical potential used in this work and the results of CMD simulations with the empirical potential are summarized in the Supporting Information.

To confirm the quality of the ANN potential for energies and structures, first the total energies produced by the ANN potential were compared with the corresponding reference energies obtained from FPMD (Figure 2a). We can clearly see that the ANN potential provides accurate potential energy not only for the atomic configurations of the training data set but also those for test data set. The final root-mean-square errors (RMSEs) of the training and test sets were about 0.6 and 0.7 meV/atom, corresponding to temperatures of 6 and 7 K, respectively. As the temperature increased to more than 1000 K and in some cases exceeded 2000 K when plastic deformation occurred in the FPMD simulations, these RMSEs should be small enough.

Next, to confirm that the ANN potential provides accurate structural properties, the pair distribution functions (PDFs) of an unshocked state were calculated using the *NPT* ensemble under ambient conditions. In order to test the quality of the ANN potential for structural properties more rigidly, an additional FPMD simulation for 3000 steps (∼3.63 ps) was carried out, and the PDF was calculated with these 3000 configurations that were not used for the training of the ANN potential. ANN-MD and CMD simulations were also carried out for 4500 steps, and PDFs were calculated using configurations of the last 3000 steps. The calculated PDFs for FPMD and ANN-MD are compared in Figure 2b (the CMD result is shown in Figure S1 in the Supporting Information). The major peak positions in the ANN-MD result show good agreement with those in the FPMD result, and the overall trends also consistent with each other. Even though the reference FPMD data calculated under unshocked ambient conditions were less than 6% of all reference data, the ANN potential provided structural properties very well. In the MD simulations for unshocked ambient conditions, the computational speeds were also compared with each other. With the same number of cores (in this study, 96 cores) for the computation, the computational time of ANN-MD was more than 5000 times shorter than that of FPMD and about 7 times longer than that of CMD. This result suggests that ANN-MD may bear long-term simulations such as submicrosecond simulations for systems with several hundred particles. To summarize the analysis thus far, the ANN potential created in this work can be expected to reproduce the energetic and structural properties with high accuracy, at least for the reference structures, with a dramatic reduction of the computational costs.

Then we analyzed correlations of particle velocity with shock speed (Figure 3a) and pressure with specific volume (Figure 3b) obtained from the shock simulations of FPMD and ANN-MD.

https://dx.doi.org/10.1021/acs.jpclett.0c00637
J. Phys. Chem. Lett. 2020, 11, 4536−4541

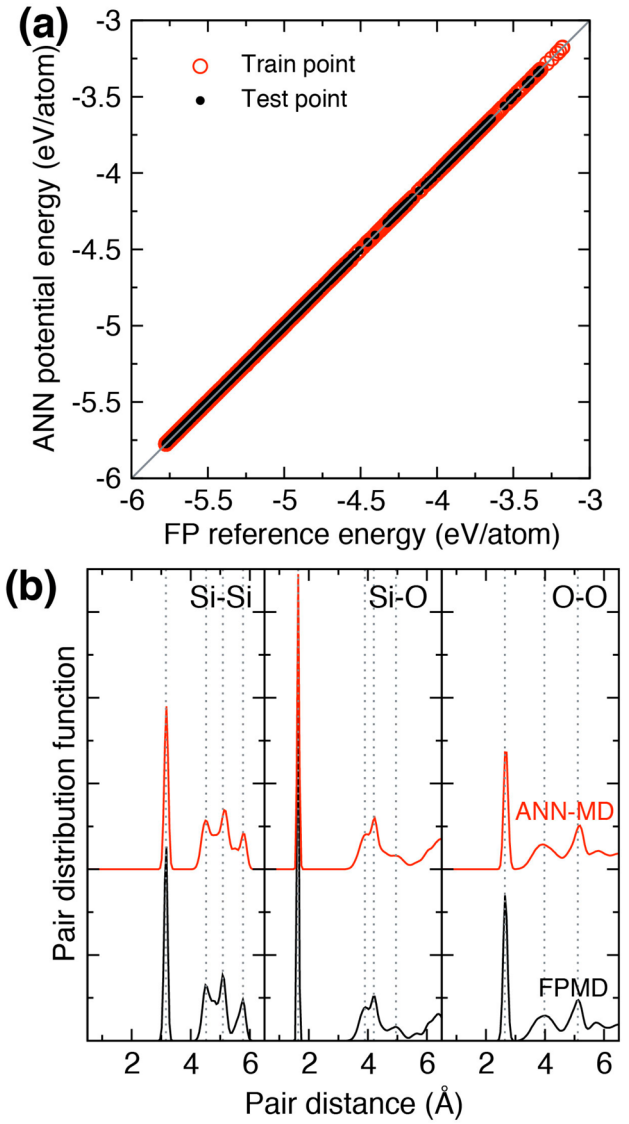

Figure 2. (a) Comparison of the potential energy predicted by the ANN potential with corresponding potential energy in the FPMD simulation. The red and black symbols indicate the potential energies for the training and test data sets, respectively. The gray line is the ideal diagonal line that shows to the location of zero-error points. (b) Pair distribution functions (PDFs) of the unshocked state under ambient conditions calculated by FPMD (black) and ANN-MD (red). The left, middle, and right sides display the PDFs for Si−Si, Si−O, and O−O pairs, respectively. The gray dotted lines indicate the positions of major peaks in the FPMD results.

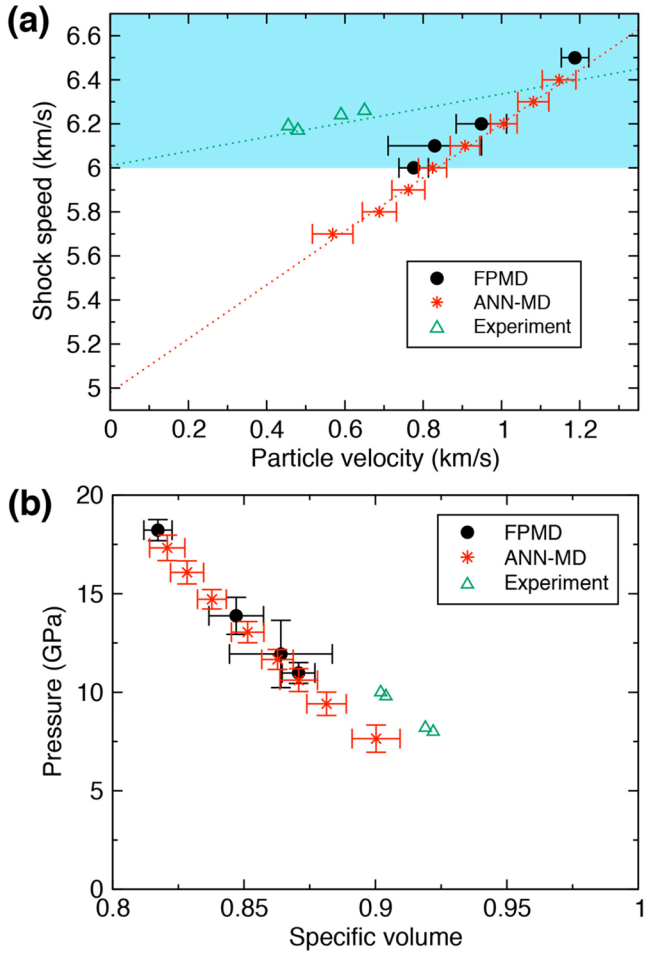

Figure 3. (a) Particle velocity vs shock speed and (b) pressure vs specific volume calculated for the shock-induced simulations. The black circles and red stars show the FPMD and ANN-MD results, respectively. The green triangles in (b) are experimental data reported by Wackerle.[31] The red and green dotted lines in (a) are the least-squares fits for the ANN-MD and experimental data, respectively. The blue highlighted area in (a) indicates the shock speed region where the FPMD method exhibits elastic deformation behavior. The error bars indicate standard deviations.

The values plotted in the figures were calculated by average in 1.21 ps for FPMD and 24.2 ps for ANN-MD and CMD. We can see that the elastic properties obtained from ANN-MD are in good agreement with the FPMD results. Here we focus on the shock speed range for the FPMD and ANN-MD methods. In the FPMD simulations, elastic deformation behavior cannot be observed for shock speeds less than 6.0 km/s on reasonable simulation time scales. The blue highlighted area in Figure 3a indicates the shock speed range that was able to reproduce elastic deformation behavior by the FPMD method. On the other hand, even though the FPMD data used in the learning process correspond to shock speeds above 6.0 km/s, ANN-MD provided reasonable results for the lower-shock-speed region (outside of the blue highlighted area). The maximum shock speed in the elastic region is a little different between the FPMD and ANN-MD results, but the particle velocities are in good agreement with each other. However, as shown with green triangles, the calculated data exhibit a different trend from the experimental data for *y*-cut quartz.[31] On the basis of the least-squares fits for the ANN-MD and experimental data (dotted lines), the difference in the expected elastic wave velocities at ambient pressure is about 1 km/s. That is, the model error of the FPMD+MSST method to describe the relation of particle velocity and shock speed is larger than the statistical error. This model error may be ascribed to the approximate exchange−correlation functional. On the other hand, the experimentally measured pressure−volume relations above the specific volume of 0.8 along the shock compression of *y*-cut quartz[31] are also plotted as green triangles in Figure 3b. We can see that our simulations represent the experimental pressure−volume correlations well. However, the highest pressures in the first elastic wave region obtained in our simulation are higher than the experimental result. It is considered that surface effects or structural defects existing under the experimental conditions

https://dx.doi.org/10.1021/acs.jpclett.0c00637
J. Phys. Chem. Lett. 2020, 11, 4536−4541

caused this difference. To demonstrate the effects of the functional on the shock compression properties, the particle velocity versus shock speed and pressure versus specific volume obtained from CMD simulations and FPMD simulations using an exchange−correlation energy functional based on the local density approximation (LDA) are shown in Figure S2.

Finally, Figure 4 shows the time evolution of the particle velocity calculated by ANN-MD shock simulations during 60.5 ps. For the shock speed range from 5.7 to 6.4 km/s, we observed elastic deformation behaviors of α-quartz. With the FPMD method, shock propagation behaviors could not be observed directly for shock speeds lower than 6.1 km/s during a reasonable computational time. On the other hand, with the ANN-MD method, elastic deformation was observed for shock speeds less than 6.1 km/s by long-term simulations for several tens of picoseconds. Such delayed convergence of the particle velocity is inherent in MSST, which to date has precluded the application of FPMD+MSST to low-speed shock. This simulation result clearly demonstrates that the ANN potential enabled shock-induced structural deformation reactions under low-shock speed conditions to be represented. The same trend is also observed for not only the time evolution of the particle velocity but also that of the uniaxial pressure and specific volume (Figure S3). The convergence values of those quantities are clearly proportional to the shock speed, as shown in Figure 3a, and it appears that reasonable behavior was produced. To summarize, the shock simulation results show that the ANN potential is able to represent the elastic shock wave simulations for a long time with first-principles accuracy.

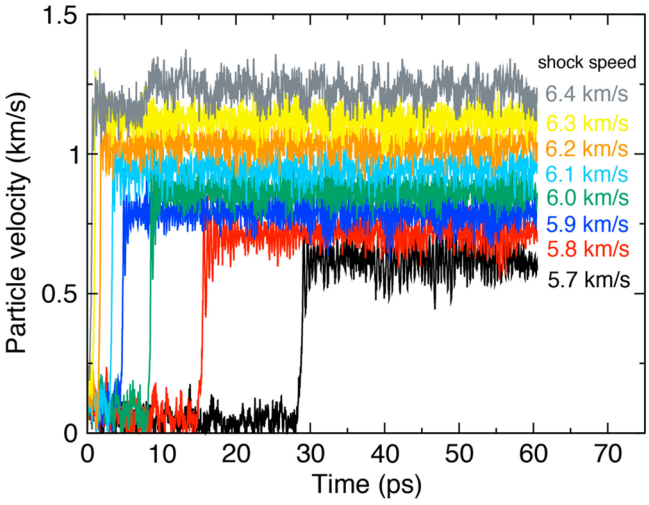

Figure 4. Time evolution of the particle velocity obtained from ANN-MD. The black, red, blue, green, cyan, orange, yellow, and gray colors indicate results for shock speeds of 5.7, 5.8, 5.9, 6.0, 6.1, 6.2, 6.3, and 6.4 km/s, respectively.

In this work, we constructed an ANN potential and performed shock simulations by ANN-MD for α-quartz. The created ANN potential provides reasonable results for energetic and structural properties in unshocked MD simulations, while the computational time is more than 5000 times shorter than for the FPMD simulation. In the shock simulation with this ANN potential, elastic deformation behaviors of α-quartz were observed with reasonable particle velocity versus shock speed and pressure versus volume correlations. In addition to that, the obtained highest pressure in the elastic region is also consistent with the FPMD and CMD results. Furthermore, deformation behaviors that take several tens of picoseconds were observed in the ANN-MD results. The FPMD method is not suitable to represent this slow reaction because of its high computational cost. Those results show that ANN-MD is able to apply the research on elastic wave propagation in solid materials and has a potential application to more complex plastic wave, shear wave, and double shock wave propagations. Moreover, our results suggest that the ANN potential can readily be applied to systems with more than two components because the Chebyshev descriptor that we employed in this work is applicable to multicomponent systems. We are confident that the powerful and efficient ANN potentials will accelerate research on the elastic properties of complex materials[32−34] and will advance into the research field of condensed matter physics under extreme conditions in the future.

COMPUTATIONAL DETAILS

In this study, all of the FPMD simulations were carried out using the QXMD code,[35,36] which is scalable parallel software for FPMD with various extensions, including omnidirectional MSST.[11] The electronic states in shock-induced α-quartz were calculated using the projector augmented-wave (PAW) method within the framework of DFT.[37] In order to represent the exchange−correlation energy, the Perdew−Burke−Ernzerhof (PBE) functional based on the generalized gradient approximation (GGA) was employed.[38] As the valence states, 3s, 3p, and 3d states for Si atoms and 2s and 2p states for O atoms were treated. The plane-wave cutoff energies were 30 and 250 Ry for the wave function and electron density, respectively. The Γ point only was used for Brillouin zone sampling. Equations of motion were solved via an explicit reversible integrator with a time step of 1.21 fs.[39]

To construct the ANN potential for the shock simulation of α-quartz, the ænet package was used for the training process.[22] The potential energies were only used for the potential fitting. The total size of the learning data set was about 23 000, including not only shock simulation data but also *NPT* relaxation processes. Both elastic and plastic deformation structures were included in the shock simulation data. In this work, as the fitting algorithm, the Levenberg−Marquardt method was employed. We used a neural network consisting of three hidden layers with 15 nodes for each layer. The "hyperbolic tangent with linear twisting" form given in ref 22 was selected as the activation function. The ratio of data for the training and test sets was set to 5:1. We employed the Chebyshev descriptor as the basis function, as suggested by Artrith et al.[23] The other detailed parameters are summarized in Table S1. With these conditions, the ANN potential was constructed using 800 iterations.

ASSOCIATED CONTENT

Supporting Information

(PDF) The Supporting Information is available free of charge at https://pubs.acs.org/doi/10.1021/acs.jpclett.0c00637.

Pair distribution functions, including the results of CMD simulations; Hugoniot relations, including the results of LDA-FPMD and CMD simulations; time evolution of the pressure and specific volume obtained from ANN-MD; and parameters for the Levenberg−Marquardt method and basis functions used in the potential training (PDF)

https://dx.doi.org/10.1021/acs.jpclett.0c00637
J. Phys. Chem. Lett. 2020, 11, 4536−4541

AUTHOR INFORMATION

Corresponding Author

Masaaki Misawa − *Graduate School of Natural Science and Technology, Okayama University, Okayama 700-8530, Japan;* orcid.org/0000-0001-7335-5046; Email: misawa@okayama-u.ac.jp

Authors

Shogo Fukushima − *Department of Physics, Kumamoto University, Kumamoto 860-8555, Japan*

Akihide Koura − *Department of Physics, Kumamoto University, Kumamoto 860-8555, Japan*

Kohei Shimamura − *Department of Physics, Kumamoto University, Kumamoto 860-8555, Japan;* orcid.org/0000-0003-3235-2599

Fuyuki Shimojo − *Department of Physics, Kumamoto University, Kumamoto 860-8555, Japan*

Subodh Tiwari − *Collaboratory for Advanced Computing and Simulations, University of Southern California, Los Angeles, California 90089, United States;* orcid.org/0000-0002-5516-6900

Ken-ichi Nomura − *Collaboratory for Advanced Computing and Simulations, University of Southern California, Los Angeles, California 90089, United States*

Rajiv K. Kalia − *Collaboratory for Advanced Computing and Simulations, University of Southern California, Los Angeles, California 90089, United States*

Aiichiro Nakano − *Collaboratory for Advanced Computing and Simulations, University of Southern California, Los Angeles, California 90089, United States;* orcid.org/0000-0003-3228-3896

Priya Vashishta − *Collaboratory for Advanced Computing and Simulations, University of Southern California, Los Angeles, California 90089, United States;* orcid.org/0000-0003-4683-429X

Complete contact information is available at: https://pubs.acs.org/10.1021/acs.jpclett.0c00637

Notes

The authors declare no competing financial interest.

ACKNOWLEDGMENTS

This study was supported by JST CREST Grant JPMJCR18I2 and JSPS KAKENHI Grant 20K14378. The work at the University of Southern California was supported as part of the Computational Materials Sciences Program funded by the U.S. Department of Energy, Office of Science, Office of Basic Energy Sciences, under Award DE-SC0014607. The authors thank the Supercomputer Center at the Institute for Solid State Physics, University of Tokyo, for the use of the facilities. Simulations were also carried out using the facilities of the Research Institute for Information Technology, Kyushu University.

REFERENCES

(1) Shen, Y.; Jester, S. B.; Qi, T.; Reed, E. J. Nanosecond Homogeneous Nucleation and Crystal Growth in Shock-Compressed SiO_2. *Nat. Mater.* **2016**, *15*, 60−65.

(2) Kubo, T.; Kato, T.; Higo, Y.; Funakoshi, K. Curious Kinetic Behavior in Silica Polymorphs Solves Seifertite Puzzle in Shocked Meteorite. *Sci. Adv.* **2015**, *1*, No. e1500075.

(3) Panero, W. R.; Benedetti, L. R.; Jeanloz, R. Equation of State of Stishovite and Interpretation of SiO_2 Shock-Compression Data. *J. Geophys. Res.: Solid Earth* **2003**, *108*, ECV 5.

(4) Mundy, C. J.; Curioni, A.; Goldman, N.; Kuo, I. F. W.; Reed, E. J.; Fried, L. E.; Ianuzzi, M. Ultrafast Transformation of Graphite to Diamond: An Ab Initio Study of Graphite Under Shock Compression. *J. Chem. Phys.* **2008**, *128*, 184701.

(5) Gleason, A. E.; Bolme, C. A.; Lee, H. J.; Nagler, B.; Galtier, E.; Milathianaki, D.; Hawreliak, J.; Kraus, R. G.; Eggert, J. H.; Fratanduono, D. E.; et al. Ultrafast Visualization of Crystallization and Grain Growth in Shock-Compressed SiO_2. *Nat. Commun.* **2015**, *6*, 8191.

(6) Nishiyama, N.; Wakai, F.; Ohfuji, H.; Tamenori, Y.; Murata, H.; Taniguchi, T.; Matsushita, M.; Takahashi, M.; Kulik, E.; Yoshida, K.; et al. Fracture-Induced Amorphization of Polycrystalline SiO_2 Stishovite: a Potential Platform for Toughening in Ceramics. *Sci. Rep.* **2015**, *4*, 6558.

(7) Yoshida, K.; Wakai, F.; Nishiyama, N.; Sekine, R.; Shinoda, Y.; Akatsu, T.; Nagoshi, T.; Sone, M. Large Increase in Fracture Resistance of Stishovite with Crack Extension Less than One Micrometer. *Sci. Rep.* **2015**, *5*, 10993.

(8) Yoshida, K.; Nishiyama, N.; Sone, M.; Wakai, F. Strength and Toughness of Nanocrystalline SiO_2 Stishovite Toughened by Fracture-Induced Amorphization. *Acta Mater.* **2017**, *124*, 316−324.

(9) Misawa, M.; Ryuo, E.; Yoshida, K.; Kalia, R. K.; Nakano, A.; Nishiyama, N.; Shimojo, F.; Vashishta, P.; Wakai, F. Picosecond Amorphization of SiO_2 Stishovite under Tension. *Sci. Adv.* **2017**, *3*, No. e1602339.

(10) Reed, E. J.; Fried, L. E.; Joannopoulos, J. D. A Method for Tractable Dynamical Studies of Single and Double Shock Compression. *Phys. Rev. Lett.* **2003**, *90*, 235503.

(11) Shimamura, K.; Misawa, M.; Ohmura, S.; Shimojo, F.; Kalia, R. K.; Nakano, A.; Vashishta, P. Crystalline Anisotropy of Shock-Induced Phenomena: Omni-Directional Multiscale Shock Technique. *Appl. Phys. Lett.* **2016**, *108*, No. 071901.

(12) Shimamura, K.; Misawa, M.; Li, Y.; Kalia, R. K.; Nakano, A.; Shimojo, F.; Vashishta, P. A Crossover in Anisotropic Nanomechanochemistry of Van Der Waals Crystals. *Appl. Phys. Lett.* **2015**, *107*, 231903.

(13) Ge, N. N.; Wei, Y. K.; Song, Z. F.; Chen, X. R.; Ji, G. F.; Zhao, F.; Wei, D. Q. Anisotropic Responses and Initial Decomposition of Condensed-Phase β-HMX under Shock Loadings via Molecular Dynamics Simulations in Conjunction with Multiscale Shock Technique. *J. Phys. Chem. B* **2014**, *118*, 8691−8699.

(14) Shimojo, F.; Hattori, S.; Kalia, R. K.; Kunaseth, M.; Mou, W. W.; Nakano, A.; Nomura, K.; Ohmura, S.; Rajak, P.; Shimamura, K.; et al. A Divide-Conquer-Recombine Algorithmic Paradigm for Large Spatiotemporal Quantum Molecular Dynamics Simulations. *J. Chem. Phys.* **2014**, *140*, 18A529.

(15) Yamada, S.; Shimojo, F.; Akashi, R.; Tsuneyuki, S. Efficient Method for Calculating Spatially Extended Electronic States of Large Systems with a Divide-and-Conquer Approach. *Phys. Rev. B: Condens. Matter Mater. Phys.* **2017**, *95*, No. 045106.

(16) Behler, J.; Lorenz, S.; Reuter, K. Representing Molecule-Surface Interactions with Symmetry-Adapted Neural Networks. *J. Chem. Phys.* **2007**, *127*, No. 014705.

(17) Behler, J.; Parrinello, M. Generalized Neural-Network Representation of High-Dimensional Potential-Energy Surfaces. *Phys. Rev. Lett.* **2007**, *98*, 146401.

(18) Artrith, N.; Morawietz, T.; Behler, J. High-Dimensional Neural-Network Potentials for Multicomponent Systems: Applications to Zinc Oxide. *Phys. Rev. B: Condens. Matter Mater. Phys.* **2011**, *83*, 153101.

(19) Behler, J. Neural Network Potential-Energy Surfaces in Chemistry: A Tool for Large-Scale Simulations. *Phys. Chem. Chem. Phys.* **2011**, *13*, 17930−17955.

(20) Jose, K. V. J.; Artrith, N.; Behler, J. Construction of High-Dimensional Neural Network Potentials Using Environment-Dependent Atom Pairs. *J. Chem. Phys.* **2012**, *136*, 194111.

(21) Behler, J. Constructing High-Dimensional Neural Network Potentials: A Tutorial Review. *Int. J. Quantum Chem.* **2015**, *115*, 1032−1050.

(22) Artrith, N.; Urban, A. An Implementation of Artificial Neural-Network Potentials for Atomistic Materials Simulations: Performance for TiO_2. *Comput. Mater. Sci.* **2016**, *114*, 135−150.
(23) Artrith, N.; Urban, A.; Ceder, G. Efficient and Accurate Machine-Learning Interpolation of Atomic Energies in Compositions with Many Species. *Phys. Rev. B: Condens. Matter Mater. Phys.* **2017**, *96*, No. 014112.
(24) Behler, J. Atom-Centered Symmetry Functions for Constructing High-Dimensional Neural Network Potentials. *J. Chem. Phys.* **2011**, *134*, No. 074106.
(25) Van Duin, A. C. T.; Dasgupta, S.; Lorant, F.; Goddard, W. A., III. ReaxFF: A Reactive Force Field for Hydrocarbons. *J. Phys. Chem. A* **2001**, *105*, 9396−9409.
(26) Nielson, K. D.; Van Duin, A. C. T.; Oxgaard, J.; Deng, W. Q.; Goddard, W. A., III. Development of the ReaxFF Reactive Force Field for Describing Transition Metal Catalyzed Reactions, with Application to the Initial Stages of the Catalytic Formation of Carbon Nanotubes. *J. Phys. Chem. A* **2005**, *109*, 493−499.
(27) Shakouri, K.; Behler, J.; Meyer, J.; Kroes, G. J. Accurate Neural Network Description of Surface Phonons in Reactive Gas-Surface Dynamics: N_2 + Ru(0001). *J. Phys. Chem. Lett.* **2017**, *8*, 2131−2136.
(28) Hellström, M.; Ceriotti, M.; Behler, J. Nuclear Quantum Effects in Sodium Hydroxide Solutions from Neural Network Molecular Dynamics Simulations. *J. Phys. Chem. B* **2018**, *122*, 10158−10171.
(29) Quaranta, V.; Hellström, M.; Behler, J.; Kullgren, J.; Mitev, P. D.; Hermansson, K. Maximally Resolved Anharmonic OH Vibrational Spectrum of the Water/ZnO(10 1 0) Interface from a High-Dimensional Neural Network Potential. *J. Chem. Phys.* **2018**, *148*, 241720.
(30) Shimamura, K.; Fukushima, S.; Koura, A.; Shimojo, F.; Misawa, M.; Kalia, R. K.; Nakano, A.; Vashishta, P.; Matsubara, T.; Tanaka, S. Guidelines for Creating Artificial Neural Network Empirical Interatomic Potential from First-Principles Molecular Dynamics Data Under Specific Conditions and Its Application to α-Ag_2Se. *J. Chem. Phys.* **2019**, *151*, 124303.
(31) Wackerle, J. Shock-Wave Compression of Quartz. *J. Appl. Phys.* **1962**, *33*, 922−937.
(32) Inui, M.; Baron, A. Q. R.; Kajihara, Y.; Matsuda, K.; Hosokawa, S.; Kimura, K.; Tsuchiya, Y.; Shimojo, F.; Yao, M.; Tsutsui, S.; et al. Viscoelastic Anomaly Accompanying Anti-Crossing Behaviour in Liquid As_2Se_3. *J. Phys.: Condens. Matter* **2018**, *30*, 28LT02.
(33) Choudhary, K.; Cheon, G.; Reed, E.; Tavazza, F. Elastic Properties of Bulk and Low-Dimensional Materials Using Van Der Waals Density Functional. *Phys. Rev. B: Condens. Matter Mater. Phys.* **2018**, *98*, No. 014107.
(34) Hsu, H.; Umemoto, K.; Wu, Z.; Wentzcovitch, R. M. Spin-State Crossover of Iron in Lower-Mantle Minerals: Results of DFT+U Investigations. *Rev. Mineral. Geochem.* **2010**, *71*, 169−199.
(35) Shimojo, F.; Kalia, R. K.; Nakano, A.; Vashishta, P. Linear-Scaling Density-Functional-Theory Calculations of Electronic Structure Based on Real-Space Grids: Design, Analysis, and Scalability Test of Parallel Algorithms. *Comput. Phys. Commun.* **2001**, *140*, 303−314.
(36) Shimojo, F.; Fukushima, S.; Kumazoe, H.; Misawa, M.; Ohmura, S.; Rajak, P.; Shimamura, K.; Bassman, L.; Tiwari, S.; Kalia, R. K.; et al. QXMD: An Open-Source Program for Nonadiabatic Quantum Molecular Dynamics. *SoftwareX* **2019**, *10*, 100307.
(37) Blöchl, P. E. Projector Augmented-Wave Method. *Phys. Rev. B: Condens. Matter Mater. Phys.* **1994**, *50*, 17953−17979.
(38) Perdew, J. P.; Burke, K.; Ernzerhof, M. Generalized Gradient Approximation Made Simple. *Phys. Rev. Lett.* **1996**, *77*, 3865−3868.
(39) Martyna, G. J.; Klein, M. L.; Tuckerman, M. Nose-Hoover Chains - the Canonical Ensemble via Continuous Dynamics. *J. Chem. Phys.* **1992**, *97*, 2635−2643.

https://dx.doi.org/10.1021/acs.jpclett.0c00637
J. Phys. Chem. Lett. 2020, 11, 4536−4541